ORIGINAL ARTICLE

Open Access

CrossMark

Experimental Investigation on Damage Behavior of Polypropylene Fiber Reinforced Concrete under Compression

Lihua Xu[1], Biao Li[1], Xiaoxiao Ding[2], Yin Chi[1*], Changning Li[1], Biao Huang[1] and Yuchuan Shi[1]

Abstract

This paper presents an experimental investigation on the stress–strain behavior and the damage mechanism of polypropylene fiber reinforced concrete (PFRC) under monotonic and cyclic compression. Fifty-four specimens for different fiber volume fractions and aspect ratios were tested. Acoustic emission (AE) technique was used to monitor the damage progression. The damage mechanism of concrete was analyzed based on the AE parametric analysis. The results show that the incorporation of polypropylene fiber (PF) has a positive effect on the monotonic and cyclic behaviors of concrete, especially for the post-cracking branch. The toughness and ultimate strain are enhanced and the performance degradation in terms of elastic stiffness and strength is alleviated by the addition of PF. However, PF has little influences on the plastic strain, and the damage process of concrete is mainly driven by the envelope strain. The effect of fiber volume fraction on the cyclic behavior of concrete shows more pronounced than that of aspect ratio. In addition, it is found from AE results that the damage, closely related to AE events, has a quick evolution just after the peak stress, with the AE hits having a concentrated release. The total amount of AE hits increases with increasing fiber volume fraction due to fiber pullout and sliding, while the concrete with fiber aspect ratio of 280 reaches the largest amount. Meanwhile, as substantiated by AE, the failure of PFRC shows an obvious shear mode, with shear cracks dominating the damage progression. Finally, a damage elasto-plastic model is developed to predict the monotonic and cyclic responses of PFRC and the prediction yields a fairly close estimation with experimental results.

Keywords: polypropylene fiber reinforced concrete, stress–strain behavior, monotonic/cyclic loading, acoustic emission (AE), damage, constitutive model

1 Background

In recent years, polypropylene fiber reinforced concrete (PFRC) has been experiencing a rapid development and its application has become widespread in civil engineering fields, such as constructions, bridges, surface of pavements, tunnel linings and hydraulic structures (Brandt 2008). It is acknowledged that the reliable design and seismic retrofit of PFRC structures against external complex actions, e.g., earthquake, fatigue and other types of loads, necessitates a clear comprehension of the

mechanical behavior of PFRC under both monotonic and cyclic loadings. Moreover, as demonstrated by experimental observations (Li and Ren 2009; Dassios et al. 2013), the failure behaviors of concrete members and structures are mainly determined by the damage accumulation during the loading process. The damage evolution law and damage mechanism at a material level are the key aspects for accurate prediction of the mechanical behavior of PFRC structures. Therefore, a good understanding of the monotonic/cyclic stress–strain behavior and damage mechanism of PFRC is of great importance for the engineering design of PFRC structures and the application of PFRC material.

Over the past decades, extensive studies on the mechanical properties of PFRC have been conducted. As reported by previous studies (Song et al. 2005;

---

*Correspondence: yin.chi@whu.edu.cn
[1] School of Civil Engineering, Wuhan University, 8 Dong Hu South Road, Wuhan 430072, China
Full list of author information is available at the end of the article

Xu *et al. Int J Concr Struct Mater*   (2018) 12:68

Page 2 of 20

Mazaheripour et al. 2011; Kakooei et al. 2012; Cifuentes and Garcfa 2013; Nili and afroughsabet 2010; Yin et al. 2015; Karahan and Atis 2011; Zhang and Li 2013), when adding polypropylene fibers (PFs) into concrete matrix, the tensile and flexure strength, impact toughness, fatigue performance and post-peak ductility as well as durability of concrete are remarkably enhanced. Moreover, many experimental efforts have been devoted to investigating the stress–strain behavior of PFRC as well as steel-polypropylene hybrid fiber reinforced concrete (HFRC) material (Alhozaimy et al. 1996; Parveen 2013; Zhang et al. 2016; Hasan et al. 2011; Libre et al. 2011; Chi et al. 2014; Caggiano et al. 2016). However, it has to be noted that, the previous studies are concentrated on the static loading case, and the mechanical behavior of PFRC under cyclic loading has not been investigated according to the author's knowledge. In regard to the material's cyclic response in vast available body of literature, considerable efforts have been carried out to deal with the mechanical behavior of plain concrete (Sinha et al. 1964; Karsan and Jirsa 1969; Yankelevsky and Rainhardt 1989; Bahn and Hsu 1988; Sinaie et al. 2015), fiber reinforced concrete (FRC) (Otter and Naaman 1988; Campione and Mendola 2001; Tangawa and Hatanaka 1983) and confined concrete (Abbasnia and Ziaadiny 2010; Wang et al. 2012; Lam et al. 2006) under cyclic compression. Empirical and theoretic models were proposed to estimate the monotonic and cyclic stress–strain responses of concrete based on test results (Suaris et al. 1990; Maekawa and EI-Kashif 2004; Breccolotti et al. 2015; Osorio et al. 2013; Neuenschwander et al. 2016; Lam and Teng 2009; He et al. 2008). The cyclic mechanical parameters such as macro strain, strength, elastic stiffness, and dissipated energy etc. were selected to characterize the damage index (Suaris et al. 1990; Maekawa and EI-Kashif 2004; Breccolotti et al. 2015; Neuenschwander et al. 2016). However, the underlying real damage process and damage mechanism of concrete cannot be revealed from the macro observations as the internal damage and microstructure evolution are induced by the propagation of initial micro-voids and micro-cracks. With the recent advances in nondestructive testing (NDT) methods, acoustic emission (AE) technique has been successfully used in monitoring the damage process and analyzing the failure mechanism of concrete (Dai et al. 2012; Watanabe et al. 2007). Abundant experimental studies on AE behavior and failure process of FRC have been conducted through a beam bending test, with the effects of different fibers (i.e. steel fiber, glass fiber, carbon fiber, polyvinyl alcohol fiber) analyzed (Soulioti et al. 2009; Lee and Lee 2002; Liang et al. 2004; Aggelis et al. 2011). The AE parametric analysis was used to assist the monitoring of the failure mode and the prediction of service

lifetime for composite reinforced concrete structures (Swit 2004; Nobili et al. 2013), while the effect of PF on the AE response of concrete at a material level has not been reported yet. For an accurate prediction and design, the authentic damage process and the true failure mechanism of PFRC material, which are of particular importance for a clear understanding of the mechanical behavior of PFRC subjected to external loads, needs a further investigation.

The objective of this paper is to study the monotonic and cyclic stress–strain behaviors and reveal the damage mechanism of PFRC. The effects of fiber volume fractions and aspect ratios are studied. The damage process of PFRC is analyzed using the macro cyclic parameters and AE results. The damage mechanism is discussed based on AE parametric analysis in terms of average frequency (AF) and rise angle (RA) value. In addition, a damage elasto-plastic constitutive model is developed to generate the monotonic and cyclic compressive stress–strain response of PFRC, which is useful in design of PFRC structures and prediction of structural responses.

2 Experimental Program
2.1 Materials and Mix Proportions
For the concrete production, ordinary Portland cement of type 42.5R was used as the binder. Gravel stones with the sizes between 5 and 20 mm and river sands with the fineness modulus of 2.6 were used as the coarse and fine aggregates, respectively. The nature water was used in the mix. A water reducer with the rate of 20% was used as the superplasticizer. The basic plain concrete mix proportion of cement:water:sand:coarse aggregate by weight was in the ratio of 1:0.42:1.74:2.60, which was designed according to the code JGJ-2011 (2011).

PF having a fixed diameter of 48 μm was used in the present study. Three lengths of 8, 13.6 and 19 mm were selected, corresponding to the aspect ratios of 167, 280 and 396. The physical and mechanical properties are shown in Table 1. According to the industrial instructions, four volume fractions of 0.05, 0.10, 0.15 and 0.20% were respectively selected. The details of specimens are given in Table 2.

2.2 Specimens Preparation
The prism specimens with a dimension of 150 mm × 150 mm × 300 mm were prepared in this study. Considering the difficult dispersion of PF, the fibers were manually scattered in the mixture during the concrete mixing procedure. The detailed mixing process is shown as follows: (1) adding dry fine aggregates and cement into the mixer, and starting the mixer for 2 min. (2) Dispersing the polypropylene fibers into the running mixer slowly by hand to ensure an excellent distribution. (3) Pouring the

Table 1 Major properties of fibers.

No.	Aspect ratio	Length (mm)	Diameter (μm)	Density (g/cm³)	Elastic modulus (GPa)	Melting point (°C)	Tensile strength (MPa)	Water absorption (%)
PFA	167	8	48	0.91	6.5	160	≥ 400	< 0.1
PFB	280	13.6						
PFC	396	19						

Table 2 Details of specimens.

No.	Specimens	V_{pf} (%)	l_{pf}/d_{pf}	f_{cu} (MPa)	f_{st} (MPa)
1	PF000	–	–	47.53	2.75
2	PFA05	0.05	167	50.62	3.24
3	PFA10	0.10	167	49.43	3.35
4	PFA15	0.15	167	48.84	3.47
5	PFA20	0.20	167	45.22	3.17
6	PFB10	0.10	280	51.26	3.42
7	PFB15	0.15	280	47.45	3.68
8	PFC10	0.10	396	50.14	3.55
9	PFC15	0.15	396	50.65	3.58

Fig. 1 Schematic diagram of test setup.

tap water and superplasticizer into the mixer, and mixing the mixture for 2 min. (4) Feeding coarse aggregates into the mixer, and then continuing for 3 min.

Once the mixing process completed, the fresh concrete was placed into plastic molds. After vibrated slowly for 3–5 min at a vibrating table until the fresh concrete compacting, the molds were kept under laboratory condition for 24 h. The specimens were then removed from the molds carefully and kept in a standard curing room with a constant temperature of 20 ± 2 °C and humidity of 95% until 28-day strength achieved. Each mixture type included six 150 mm × 150 mm × 150 mm cubic specimens for compressive strength (f_{cu}) and splitting tensile strength (f_{st}) (Table 2), six prism specimens for uniaxial monotonic and cyclic compressive loading tests. A total of 108 samples for 9 mix design protocols were prepared.

2.3 Test Setup
The uniaxial compressive loading tests were performed on a universal electro-hydraulic servo rock testing machine INSTRON-1346, which has a 2000-kN load capacity. The schematic diagram of the test setup is shown in Fig. 1. Two linear variable displacement transducers (1#, 2# LVDT) with a maximal range of 5 mm were placed to measure the vertical displacement, and the lateral displacement was monitored by 3#, 4#LVDT with a maximal range of 2.5 mm during the loading process. The axial load and displacements were recorded

automatically to the data acquisition system with a synchronized frequency of 50 Hz and stored in a computer.

Acoustic emission (AE) signals were acquired by a PCI-2 AE acquisition system produced by the American Physical Acoustics Corporation. Two Nano30 sensors (1#, 2#) were symmetrically distributed on the sample (see in Fig. 1) and the operating frequency ranges from 100 to 400 kHz. The amplitude distribution covers the range 0–100 dB. Both the preamplifier gain and the threshold of detection were set to 40 dB. The peak and hit definition times were 200 and 800 μs. The propagation speed of waves was 4286 m/s. The AE sensors were mounted through the following steps: (1) coating the couple agent-Vaseline on the AE sensors surface; (2) sticking sensors to the specimen surfaces by plastic tape; (3) checking the coupling effect between sensors and specimen by the pencil lead break (PLB) test.

2.4 Loading Procedure
Both monotonic and cyclic loads were performed in this study. A pre-loading of 75kN was applied at the beginning of each test. For monotonic loading, a displacement control method with a speed of 0.002 mm/s was used. The loading process was terminated until the concrete specimens collapsed into failure. For cyclic loading, each specimen was performed for ten loading cycles. A hierarchical loading method with a controlled displacement was adopted. In the pre-peak region (stage I), the

displacement increment in each step was 0.15 mm with the speed of 0.002 mm/s. In the post-peak region (stage II), the displacement increment was then set to 0.3 mm. Moreover, the unloading process was load controlled with a speed of 3 kN/s. The monotonic and cyclic loading schemes are shown in Fig. 2.
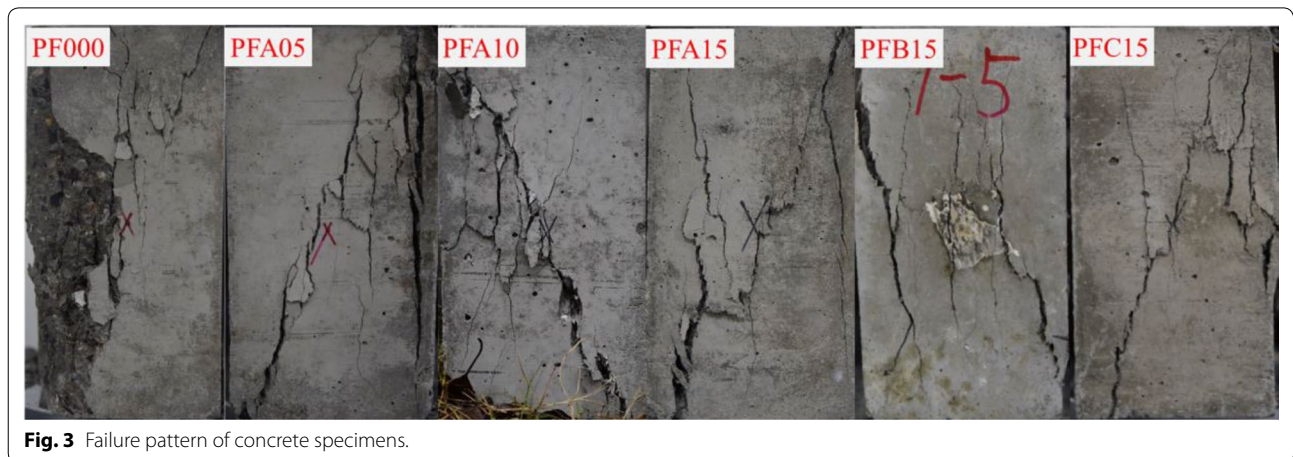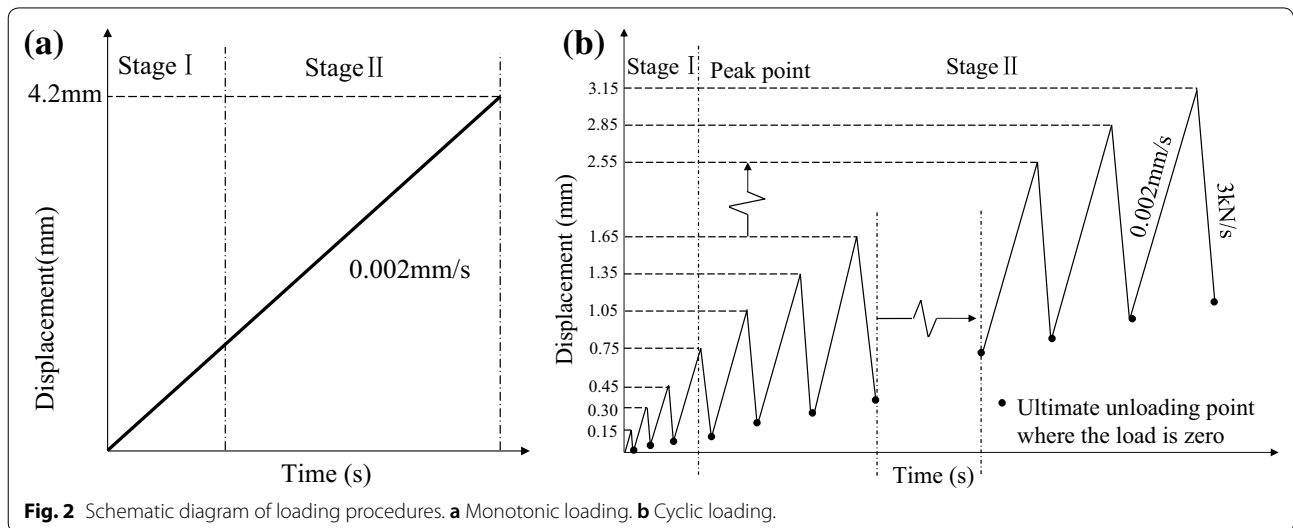
3 Results and Discussion
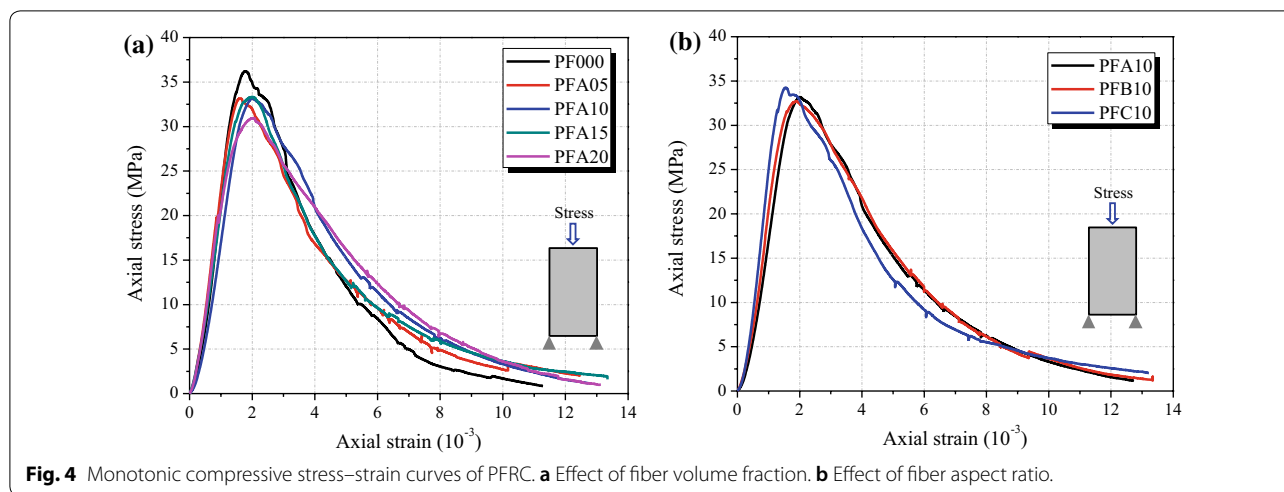
3.1 Failure Pattern
Figure 3 shows the typical failure patterns of PFRC for different mixtures, each representing a random selection from a group of three under cyclic loading. The results indicate that PF has a remarkable improvement on the failure behavior of concrete. The failure type of concrete changes from brittle failure to ductile failure by the incorporation of PF. For plain concrete, at the failure stage, large vertical cracks induced by the tensile stress perpendicular to the loading direction on the surfaces of specimens can

be seen, which slice the prismatic plain concrete specimens into small columns. While for PFRC, cross diagonal cracks appear on the surfaces of PFRC specimen, showing an obvious shear failure mode. The cracks are denser and finer, the width of which is smaller than that of plain concrete. Due to the high elongation and the large deformation of PF, fibers can bridge cracks during the failure stage. The tensile stress of a crack is transferred to the fibers, thus the fibers and concrete matrix undertake the axial loads together. When compared to plain concrete, only a few pieces of concrete spall from PFRC specimens after the peak stress. Moreover, for plain concrete, the specimen collapses into two inverted cones at the final loading stage, while for PFRC, the specimen remains integrity.

3.2 Monotonic Loading
Figure 4 shows the compressive stress–strain curves of PFRC for various fiber volume fractions and aspect

Fig. 2 Schematic diagram of loading procedures. **a** Monotonic loading. **b** Cyclic loading.

Fig. 3 Failure pattern of concrete specimens.

Fig. 4 Monotonic compressive stress–strain curves of PFRC. **a** Effect of fiber volume fraction. **b** Effect of fiber aspect ratio.

ratios under monotonic loading. Each curve represents the average results of three tests conducted at the same age and condition. The important mechanical parameters of the stress–strain curves include modulus of elasticity, peak strength, peak strain (at the maximum stress) and ultimate strain (strain where failure is defined). The tested results of each mix type from averaging a group of three are listed in Table 3. In this study, the ultimate strain is determined as a strain at the descending branch when the stress reaches 20% of the peak stress (Chen et al. 2014). The modulus of elasticity is a secant modulus taken as the slope of the chord from the origin (0 strain point) to an arbitrary point (40% of the peak stress point) on the stress–strain curve according to GB/T 50081-2002 (2002). In addition, in order to characterize and evaluate the energy dissipation capacity of concrete under monotonic compression, a compressive toughness is introduced, which is defined as the area under the stress–strain curve of concrete from the initial 0 strain and up to the ultimate strain (Chen et al. 2014). The calculated results of the compressive toughness from averaging a group of three are also shown in Table 3.

From Fig. 4, it can be seen that the stress–strain curves for different concrete mixes are similar. Overall, the ascending branches are almost tracing together until the axial stress reaches approximate 70–80% of the peak strength. The peak stress and peak strain both have a fluctuation for different fiber volume fractions and aspect ratios. The peak strength shows a slight reduction with increasing fiber volume fraction, especially when the fiber volume fraction is over 0.15%, and PF has no significant effect on the peak strain. The initial elastic modulus increases for both increasing fiber volume fraction (up to 0.15%) and aspect ratio. The increase in the fiber volume fraction ranging from 0.05, 0.10, 0.15%

increases the elastic modulus by 6.21, 8.77 and 10.64% for the constant fiber aspect ratio of 167, and the elastic modulus increases by 10.64, 11.57 and 18.80% when increasing the fiber aspect ratio from 167 to 396 with the fiber volume fraction of 0.15%. Moreover, from the figures, it is noted that PF mainly influences the descending branch of the stress–strain curve of concrete. For plain concrete, the curvature at the descending branch is larger than that of PFRC, showing a worse ductility. In general, an increase in the fiber volume fraction improves the ductile behavior of concrete. While for fiber aspect ratio, the concrete with the fiber aspect ratio of 280 shows the best ductility. In addition, the ultimate strain increases first and decreases afterwards with increasing fiber volume fractions and aspect ratios. When the volume fraction is 0.1% or the aspect ratio is 280, the concrete reaches the largest ultimate strain. An increase in the fiber volume fraction (up to 0.2%) leads to an increase in the compressive toughness by 2.12, 12.12, 15.84 and 18.55% for the four kinds of fiber volume fractions, respectively, while the toughness increases first and then decreases as the fiber aspect ratio increased (see in Fig. 5). However, when the fiber volume fraction exceeds 0.15%, a significant drop in peak strength, elastic modulus and ultimate strain is observed, which may be attributed to that incorporating a large amount of PF into concrete matrix induces more initial micro-voids and defects due to the balling effect of fibers, which thus reduces the density of the concrete composites (Kakooei et al. 2012). From the above analysis, it can be also concluded that the aspect ratio of PF has an optimum value of 280 in this study. The reason for that may be owing to that the longer fiber owns a larger embedded depth between the two sides of a crack, and thus the ultimate bond strength and the fracture resistance around a fiber

Xu *et al. Int J Concr Struct Mater*   (2018) 12:68

Page 6 of 20

Table 3 Results of compressive test under monotonic loading.

Specimen	Peak strength		Peak strain		Ultimate strain		Modulus of elasticity		Compressive toughness	
	Tested (MPa)	Ratio[a] (%)	Tested (10^{-3})	Ratio[b] (%)	Tested (10^{-3})	Ratio[c] (%)	Tested (GPa)	Ratio[d] (%)	Tested (10^{-3}MPa)	Ratio[e] (%)
PF000	36.57	0.00	1.775	0.00	6.294	0.00	2.463	0.00	121.68	0.00
PFA05	33.40	− 8.67	1.688	− 4.90	7.085	12.57	2.616	6.21	124.26	2.12
PFA10	33.66	− 7.96	1.854	4.45	7.767	23.40	2.679	8.77	136.43	12.12
PFA15	34.27	− 6.29	1.987	11.94	7.336	16.55	2.725	10.64	140.95	15.84
PFA20	29.06	− 20.54	2.016	13.58	5.586	11.25(−)	2.224	9.70f(−)	144.25	18.55
PFB10	33.12	− 9.43	1.833	3.27	7.686	22.12	2.642	7.27	139.70	14.80
PFB15	34.00	− 7.03	1.895	6.76	8.271	31.41	2.748	11.57	146.04	20.02
PFC10	34.34	− 6.10	1.765	0.56	7.029	11.68	2.730	10.84	128.26	5.41
PFC15	33.68	− 7.90	1.694	4.56	7.583	20.50	2.926	18.80	132.99	9.29

The superscripts a, b, c, d, e represent the ratio of peak strength, peak strain, ultimate strain and elastic modulus as well as energy dissipation capacity related to that of control specimen (plain concrete PF000), respectively.
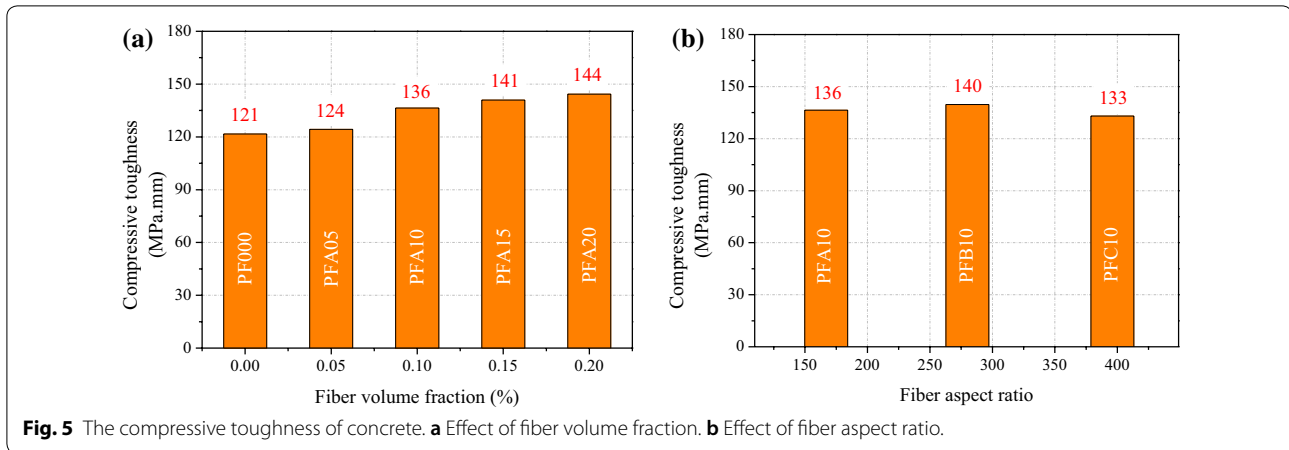
Fig. 5 The compressive toughness of concrete. **a** Effect of fiber volume fraction. **b** Effect of fiber aspect ratio.

are larger when the fiber is pulled out from a concrete matrix. On the other hand, for a constant fiber volume fraction, the specimen with a longer fiber results in a less amount of fibers in the concrete composite, thus the fiber bridging effect within cracks is generally reduced, as a result, the absorbed energy from fiber pull-out and sliding turns smaller (Huang et al. 2016).

3.3 Cyclic Loading

3.3.1 General Response

Figure 6 shows the typical cyclic stress–strain curves of PFRC for various fiber volume fractions and aspect ratios. Each curve represents a selection from a group of three. An ideal schematic of cyclic compressive process of concrete specimen extracted from the test results is shown in Fig. 7. The cyclic stress–strain response can be summarized as follows:

a. A full cycle of the stress–strain response is consisted of two distinct paths: unloading path and reloading path. The unloading path is curvilinear characterized by a progressively diminishing slope, until it intersects the strain axis. The reloading path is almost linear that starts from the strain axis and intersects the envelope curve. The nonlinearity is seen when the curve exceeds the previous envelope unloading strain, and becomes more apparent as accessing to the envelope curve (Li et al. 2017).

b. Significant degradations in elastic stiffness and stress with increasing loading cycles can be observed for all the presented cyclic stress–strain curves. The initial unloading path is almost vertical with an abrupt stress drop for a small strain increment, however, when accessing to the strain axis, the curvature of the unloading path turns larger. For the reloading path, remarkable deterioration in concrete strength can be

observed in comparison with the envelope unloading stress at the same unloading strain, which is caused by crack propagation and damage accumulation.
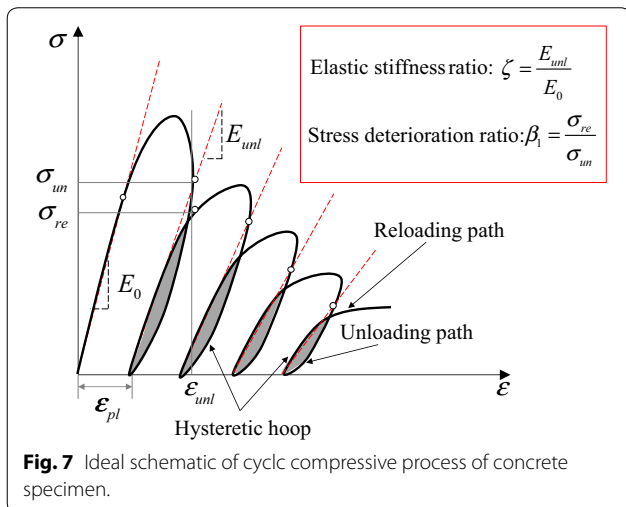
c. Prior to the peak strength, the unloading path is almost overlapping with the reloading path, and in this interval the hysteretic energy dissipation is not evident. However, in the post-peak region, the hysteretic loop becomes more obvious as the loading cycles increased. Then with increasing loading cycles, the energy dissipation capacity of concrete turns smaller or even disappears at the final loading stage. Compared to plain concrete, the hysteretic energy dissipation capacity of PFRC is stronger due to fiber sliding and pull-out mechanisms which are the main contributors to the energy dissipation.

3.3.2 Envelope Curve

The envelope curve is the upper boundary of the stress–strain response subjected to cyclic compressive loading. Previous studies on the cyclic behavior of unconfined and confined concrete have suggested a hypothesis that the monotonic stress–strain curve of a specimen can be considered as its envelope curve of the cyclic stress–strain curve (Lee and Willan 1997; Lee et al. 2014; Jin et al. 2016). In order to verify whether the hypothesis is suitable for PFRC, the envelope curve for each specimen is plotted in Fig. 6. Moreover, the monotonic stress–strain curves for the same concrete mix are also included. It can be seen that in general the monotonic stress–strain curve is lying closely to the cyclic envelope curve, with just only a small deviation. The hypothesis of envelope curve is also true for PFRC and the fiber has no influences on this hypothesis. However, it has to be mentioned that some of the monotonic stress–strain curves are worse than the cyclic ones, which can be interpreted that for monotonic loading, the stress inside the specimen increases
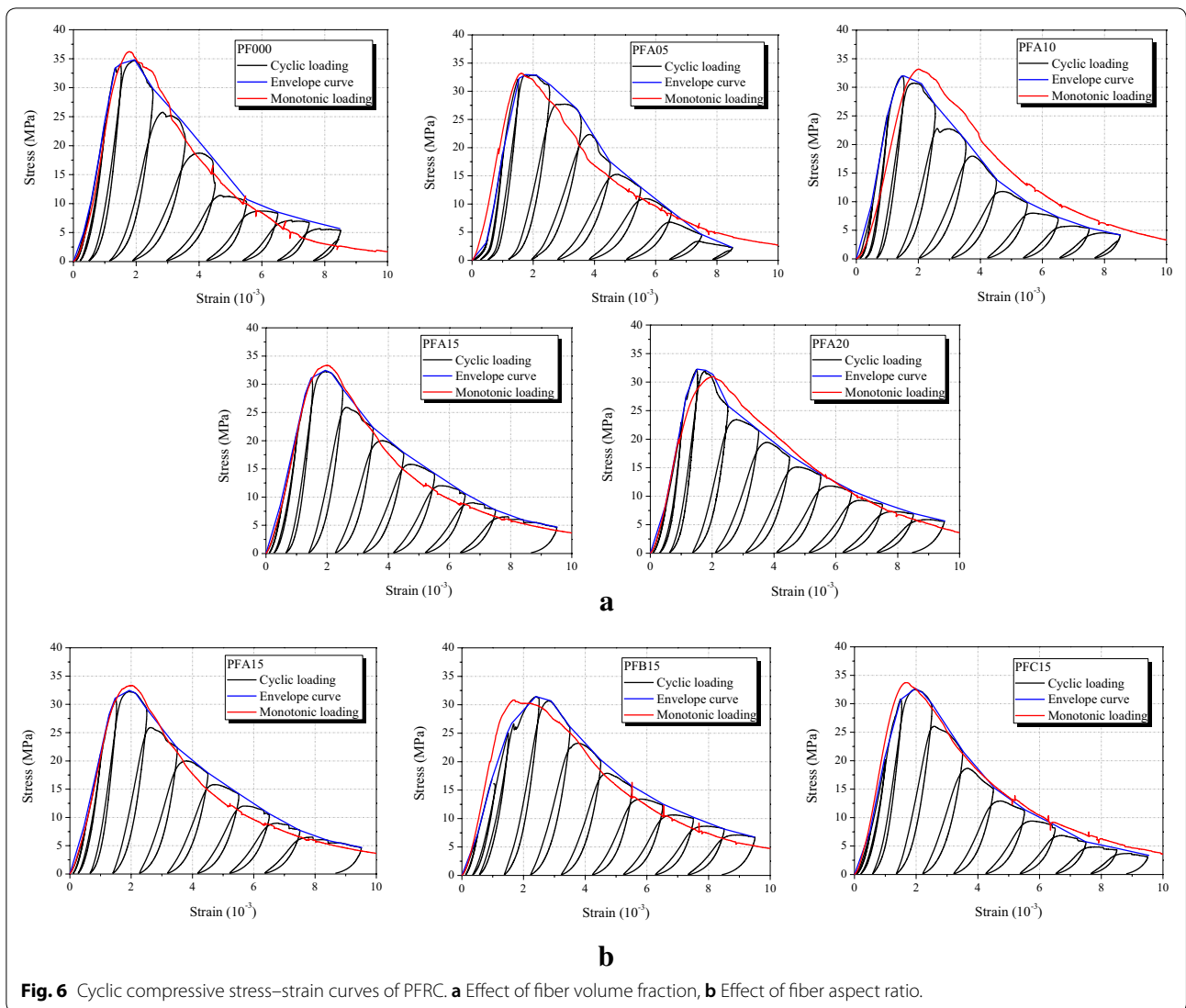
Fig. 6 Cyclic compressive stress–strain curves of PFRC. **a** Effect of fiber volume fraction, **b** Effect of fiber aspect ratio.


Elastic stiffness ratio: $\zeta = \dfrac{E_{unl}}{E_0}$

Stress deterioration ratio: $\beta_1 = \dfrac{\sigma_{re}}{\sigma_{un}}$

Fig. 7 Ideal schematic of cyclc compressive process of concrete specimen.

consecutively. There is no buffering time for the stress redistribution in the damaged specimen. However, for cyclic loading, the loading and unloading process will allow the specimen sufficient time to redistribute the stress within the undamaged microstructure of specimen. Moreover, accounting for the crack opening and closure process, the sliding and friction of the two sides of cracks would dissipate partial strain energy. In addition, the debris in the vicinity of the cracks would spall during the internal unloading–reloading cycles, which would fill the micro-pores and cracks inside the specimens, which can result in a denser microstructure of the specimen. Besides, it cannot be denied that the concrete is a high heterogeneous material. Some data discretization exists in the test results. Therefore, though at the same condition and age, the test results would be distinct and different for each concrete mixture. Based on the

above observations, the monotonic stress–strain equation of PFRC can be used to model its envelope curve under cyclic loading case.

3.3.3 Plastic Strain

Plastic strain is the residual axial strain of concrete on the unloading path when the stress is unloaded to the zero stress (Bahn and Hsu 1988; Sinaie et al. 2015). The relation between plastic strain and envelope unloading strain is one of the significant cyclic aspects (Sakai and Kawashima 2006). Figure 8 compares the plastic strain versus the envelope unloading strain for different fiber volume fractions and aspect ratios. It can be inferred that PF has a little effect on the plastic strain accumulation process of concrete. The influences of both fiber volume fraction and aspect ratio are insignificant, which are negligible in establishing the plastic strain equation. At present, various formulations for the relation of plastic strain and envelope unloading strain have been suggested,
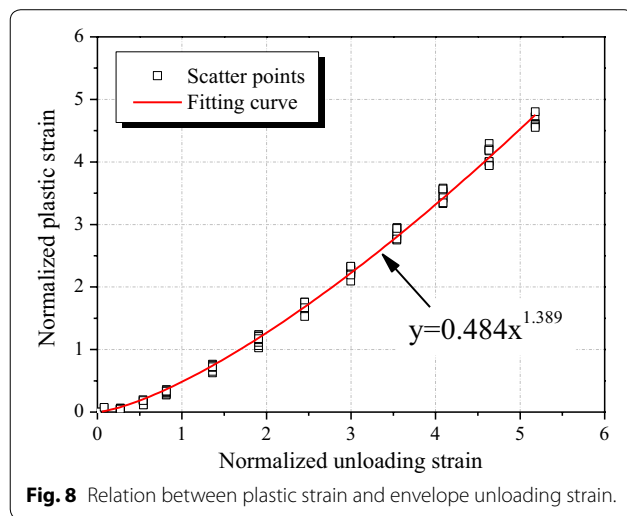
from linear to nonlinear (Bahn and Hsu 1988; Otter and Naaman 1988; Lam et al. 2006). In this study, a power function is selected to predict the relationship curve, which was firstly suggested by Bahn (Bahn and Hsu 1988) and then verified by many researchers. From a regression analysis, the equation is obtained in Eq. (1), with the effects of fibers neglected.

$$\frac{\varepsilon_{pl}}{\varepsilon_{cu}} = 0.484 \left(\frac{\varepsilon_{un}}{\varepsilon_{cu}} \right)^{1.389} \tag{1}$$
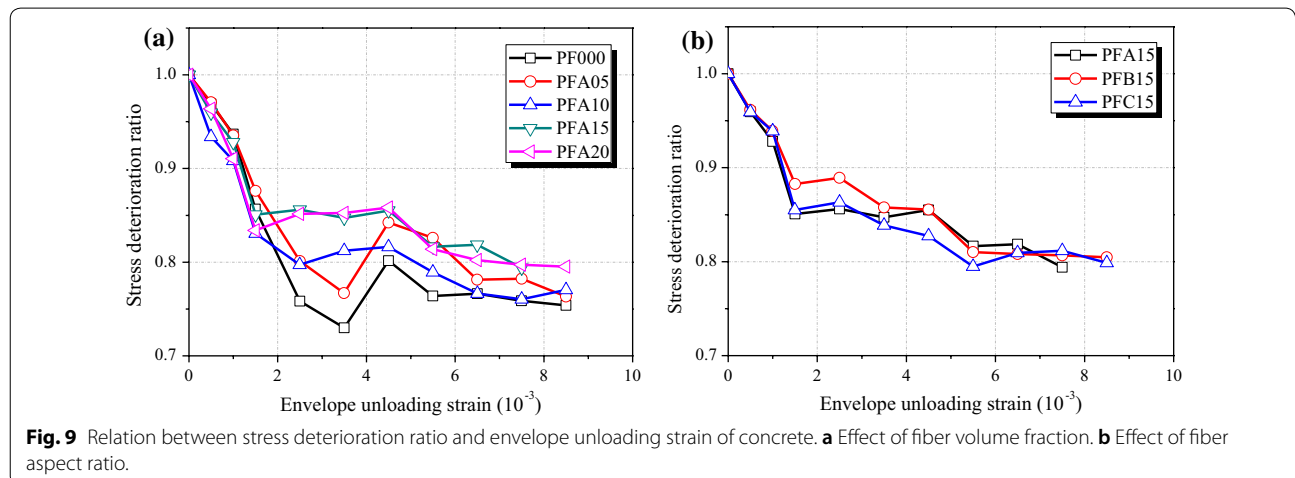
3.3.4 Stress Deterioration

Stress deterioration is an important aspect of the cyclic stress–strain behavior of concrete (Wang et al. 2012). The degree of stress deterioration for the unloading/reloading path is reflected by a stress deterioration ratio which is defined as:

$$\beta_1 = \frac{\sigma_{re}}{\sigma_{un}} \tag{2}$$

where, β_1 is the stress deterioration ratio, σ_{re} is the stress of a point on the reloading path corresponding to the first unloading strain. σ_{un} is the first envelope unloading stress.

Figure 9 shows the relation between stress deterioration ratio and envelope unloading strain for various fiber volume fractions and aspect ratios. It is found that the stress deterioration ratio is negligible when the strain is small as the concrete still remains elastic. It then decreases as the loading cycle increases, with a sharp drop almost in line before the load reaches the peak stress of concrete. After that, the stress deterioration ratio remains a constant in the subsequent loading cycles, with just a small fluctuation. It can be also inferred that PF has a significant effect on the stress

**Fig. 8** Relation between plastic strain and envelope unloading strain.

Fig. 9 Relation between stress deterioration ratio and envelope unloading strain of concrete. **a** Effect of fiber volume fraction. **b** Effect of fiber aspect ratio.

deterioration of concrete. Roughly speaking, an increase in the fiber volume fraction increases the stress deterioration ratio of concrete, especially at the peak stress regions. For fiber aspect ratio, the variable parameters seem to have insignificant effects. The specimen numbered by PFB15 obtains the slowest stress deterioration process. Therefore, it can be concluded that PF can alleviate the stress deterioration degree and then improve the ductile behavior of concrete. In addition, the effect of fiber volume fraction on the stress deterioration is more pronounced than that of fiber aspect ratio.

4 Damage
4.1 Damage Process
Figure 10 shows the typical damage process of concrete under uniaxial compression based on the elastic stiffness degradation (Fig. 10a) and AE results (Fig. 10b). It is well known that the elastic stiffness degradation is a key factor to reflect the damage degree and its evolution in concrete (Li et al. 2017; Sakai and Kawashima 2006). Herein, an elastic stiffness ratio ($E_{un,i}/E_0$) is adopted in order to study the damage process of PFRC. $E_{un,i}$ is the secant stiffness for each loading cycle, which is taken as
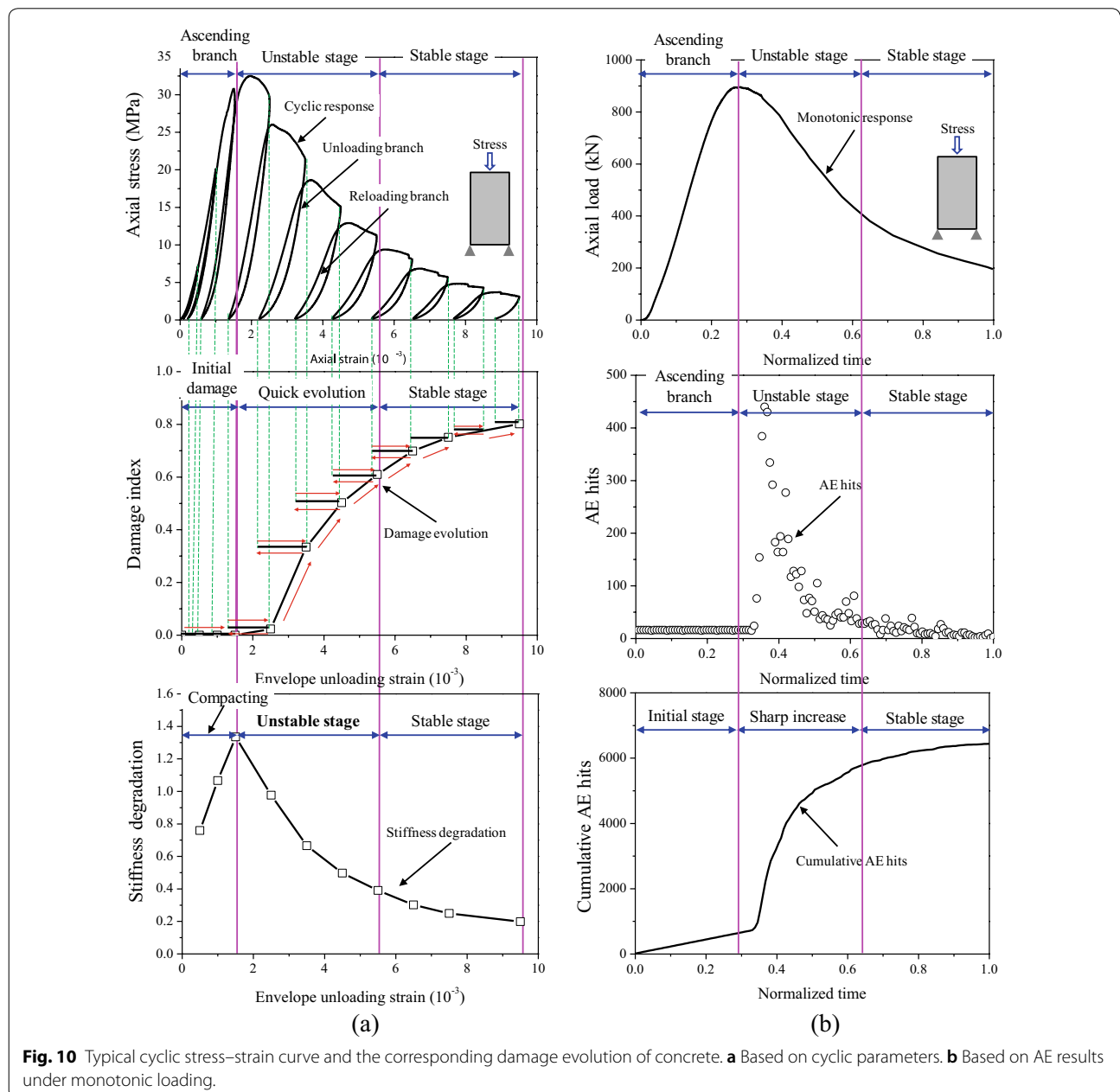
Fig. 10 Typical cyclic stress–strain curve and the corresponding damage evolution of concrete. **a** Based on cyclic parameters. **b** Based on AE results under monotonic loading.

the slope from envelope unloading point to plastic strain point on the unloading path (GB/T 50081-2002). E_0 is the initial secant elastic modulus of concrete which is obtained from averaging the results of three tested specimens under monotonic compression. Moreover, the AE phenomenon is induced by the elastic waves closely related to the crack propagation and damage evolution in a material (Dai et al. 2012). The AE behavior can be used to qualitatively characterize the damage process of concrete. The usually used AE parameters are AE hits, counts, rise time, duration time, amplitude, average frequency (AF) and rise angle (RA) value etc., which are all defined in Fig. 11a.

Figure 10a shows the typical cyclic stress–strain curve of PFRC numbered by PFA15. The elastic stiffness degradation process and the corresponding damage evolution process of concrete based on the elastic stiffness degradation process are also illustrated. Moreover, the damage indexes at the internal cycles are included. As a simplified calculation, the assumption that the damage index remains as a constant during the unloading and reloading branch is adopted (Breccolotti et al. 2015). It should be noted that due to the initial increase in elastic stiffness, the calculated damage index is negative, which violates the definition of damage. Therefore, at the first three loading cycles, the damage index is supposed as 0. It can be observed from the figure that the damage process of concrete can be divided into the following three stages:

Initial undamaged stage (about the first three loading cycles) At this stage, the damage index is accessing to 0. The concrete is still elastic. The elastic stiffness ratio increases with increasing envelope strain. The reason for that is owing to the step-by-step increased axial compressive loads make the concrete denser, with the initial micro-voids collapsed and the cracks closed. The maximum axial stress is about only 70–80% of the compressive strength of concrete, the propagation of cracks has not induced the degradation in macro elastic stiffness of concrete.

Sharp damage increasing stage (during 3–7 loading cycles) At this stage, the concrete specimen reaches the maximum density, the micro cracks start to propagate and the damage index initially increases, which induces a decrease in the elastic stiffness ratio. After the peak stress, the damage evolves quickly in the form of alike a power function, with unstable propagation of the cracks. The reduction in elastic stiffness of concrete is the fastest. At this stage, the cracks inside the concrete specimens propagate promptly, with the crack width turning larger, which damages the instinct mechanical properties of concrete significantly.

Stable damage stage (after the seventh loading cycles) When reaching the seventh loading cycle, the main damage almost has been evolved completely. The cyclic stress–strain curve is stable, with the axial stress decreasing at a slow speed. The stiffness ratio remains a constant tendency. At this stage, only the main macro cracks of concrete specimen propagate slowly. The damage energy has all been dissipated, with the damage index accessing to 1.0.

In addition, it is also observed that on the unloading path, the damage index remains a constant, with the occurrence of crack closure. On the reloading path, before the strain reaching the previous envelope unloading strain, the damage is still a constant. However, once the strain exceeds the unloading strain, the damage propagation occurs continuously with envelope strain. From the above analysis, it is noted that the damage under cyclic loading is mainly driven by the strain of envelope curve (see in Fig. 10a), which is consistent with that under monotonic loading.
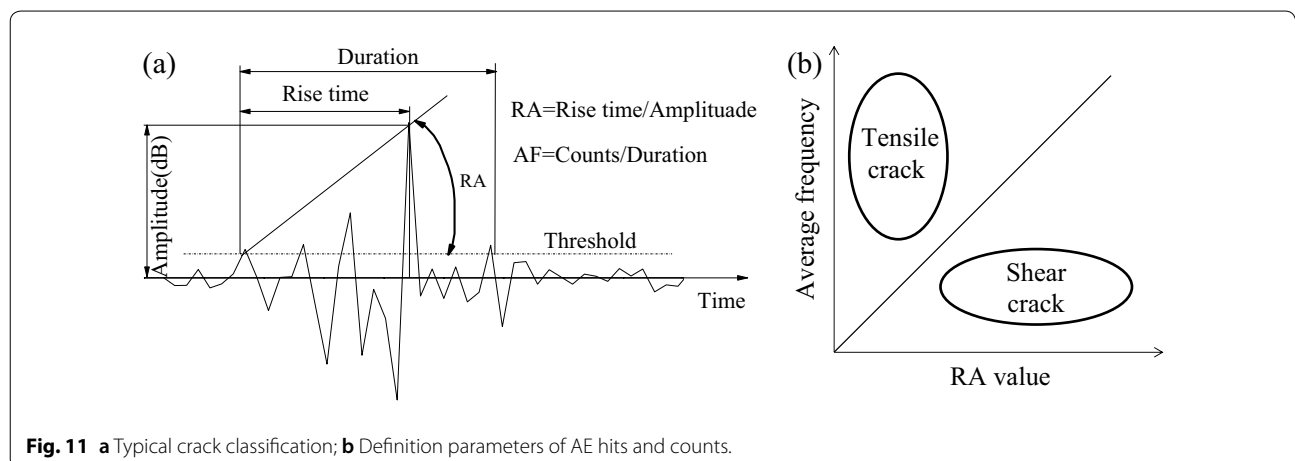

Fig. 11 **a** Typical crack classification; **b** Definition parameters of AE hits and counts.

Xu *et al. Int J Concr Struct Mater* (2018) 12:68

Page 12 of 20

Figure 10b shows the relation between AE hits and stress level under monotonic compression. The relation of the cumulative AE hits versus the normalized time is plotted in Fig. 10b. It is noted that the AE hits increase first at a slow rate before the stress reaches the peak strength. At this interval, only few AE signals are captured by the sensors. However, when the stress reaches the peak stress, a large amount of AE hits are observed accounted for the unstable crack propagation. The AE signals have a concentrated release, with the cracks in concrete specimen generating, nucleating, intersecting and finally forming into the main cracks. After the peak stress, a sharp increase in AE hits is observed. The damage at this stage has a very quick development, with an obvious decrease in the axial load. After that, the AE hits are few, resulted in a slow increase in the cumulative AE hits. The damage of concrete specimen at this interval is mainly caused by the main cracks and the damage index

at this stage is verging to a constant approaching to one. From the above analysis, it is noted that the releasing process of AE signals is closely related to the damage process of concrete. Roughly speaking, the variation process of the cumulative AE hits can be used to represent the damage evolution of concrete.

4.2 Effects of Fiber Parameters on Damage Process of PFRC
4.2.1 Stiffness Degradation
Figure 12 shows the relation between elastic stiffness ratio and envelope unloading strain of specimens. The calculated results of the elastic stiffness at each loading cycle for each concrete mix are listed in Table 4. It can be seen that PF has a positive effect on the stiffness degradation process. An increase in the fiber volume fraction leads an increase in the elastic stiffness ratio, indicating a slow stiffness degradation process. While the stiffness ratio increases first and reduces afterward with
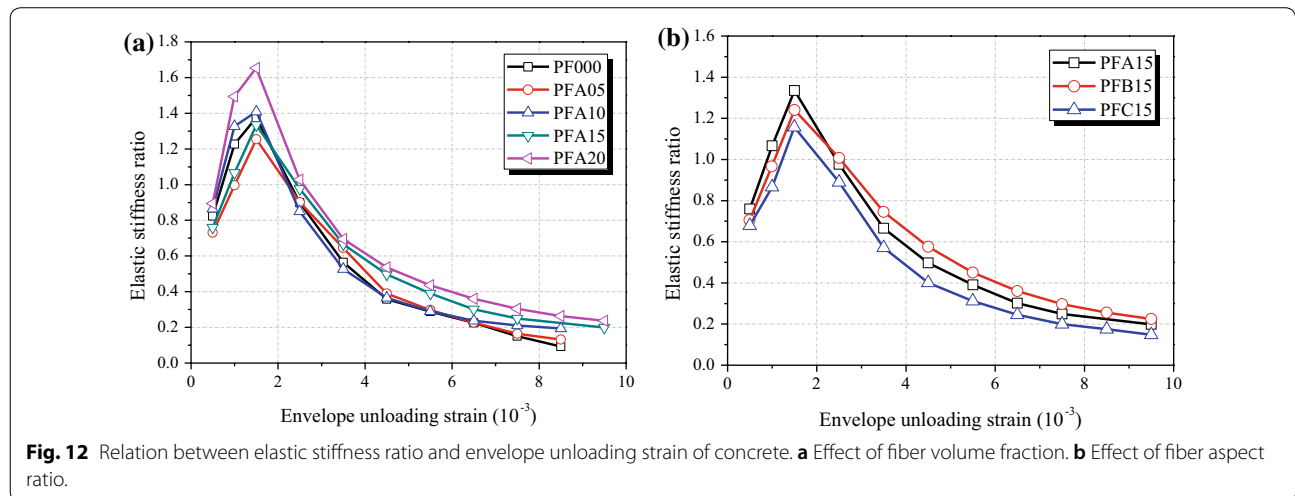
Fig. 12 Relation between elastic stiffness ratio and envelope unloading strain of concrete. **a** Effect of fiber volume fraction. **b** Effect of fiber aspect ratio.

**Table 4 Elastic stiffness of every loading cycle for each concrete mix ($\times 10^4$ MPa).**

Cycles	PF000	PFA05	PFA10	PFA15	PFB15	PFC15	PFA20
0	24.63	26.16	26.79	27.25	27.48	29.26	22.24
1	20.28	19.13	23.17	20.69	19.37	19.87	19.90
2	30.23	26.08	35.54	29.05	26.54	25.33	33.22
3	33.84	32.80	37.77	36.37	36.83	33.86	36.79
4	22.12	23.57	22.78	26.61	27.67	26.03	22.86
5	13.91	16.88	14.10	18.15	20.49	16.71	15.47
6	8.83	10.18	9.78	13.55	15.82	11.72	11.93
7	7.11	7.76	7.77	10.63	12.37	9.11	9.72
8	5.55	5.93	6.35	8.21	9.89	7.18	8.01
9	3.72	4.30	5.65	6.79	8.17	5.84	6.78
10	2.28	3.43	5.19	5.41	7.03	5.13	5.87
11	9.13	–	–	–	6.18	4.32	5.26

increasing fiber aspect ratio. The specimen PFB15 shows the slowest stiffness degradation process on the descending branch (see in Fig. 12b).

The damage evolution process of specimens is shown in Fig. 13. It can be observed that the damage evolution process for various fiber parameters is just the opposite to that of elastic stiffness degradation process. However, it has to be mentioned that due to the negligible influences of PF on the plastic strain, the elastic stiffness degradation process is mainly determined by the envelope unloading stress (see in Fig. 14). Therefore, it is further illustrated that the damage process of PFRC is just driven by the strain of envelope curve in this study.

4.2.2 Cumulative AE Hits

The cumulative AE hits versus normalized time for different fiber volume fractions and aspect ratios are shown in Fig. 15a, b. It can be observed that at the pre-peak stage, the evolution of the AE hits for various fiber parameters are almost the same. However, after the peak stress, the larger fiber volume fraction induces more AE hits. The total cumulative AE hits increase with increasing fiber volume fraction, whilst the total amount of AE hits increases first and decreases afterward when the fiber aspect ratio changes from 167 to 396, and the concrete with the aspect ratio of 280 obtains the largest amount of cumulative AE hits. The reasons are given as following: (1) for PFRC, the AE signals are mainly induced by matrix cracking, aggregate-matrix interface debonding, fiber pull-out, sliding and fracturing events, and the fiber pull-out and sliding events are proportional to the fiber volume fraction (Soulioti et al. 2009); (2) for plain concrete, only matrix cracking and aggregate-matrix interface debonding would cause AE signals, thus the total AE hits of PFRC are more than those of plain concrete, which increase as the fiber volume fraction increases; (3) for
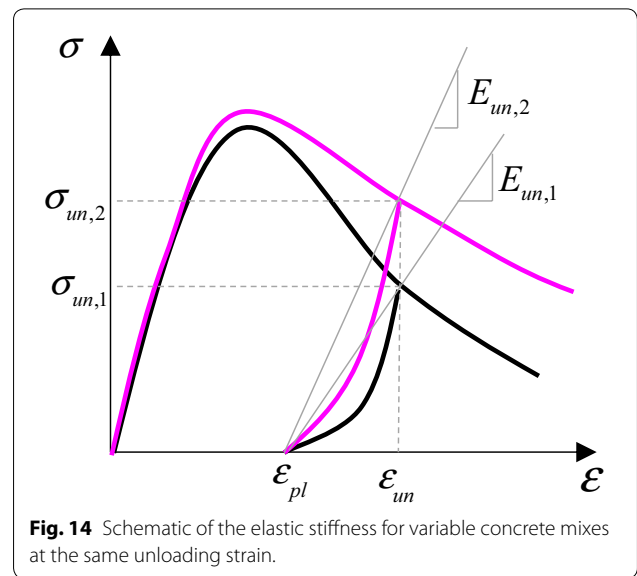
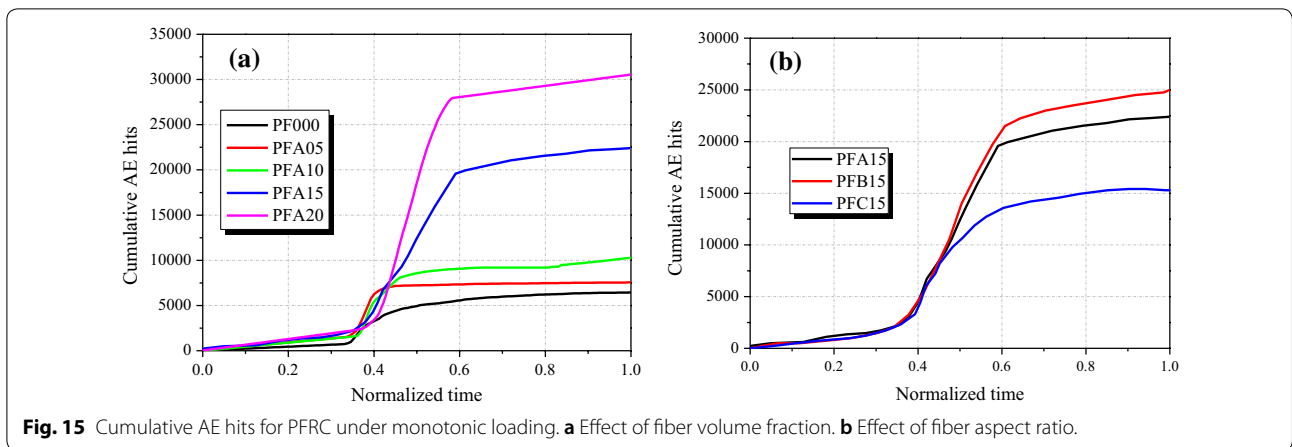**Fig. 14** Schematic of the elastic stiffness for variable concrete mixes at the same unloading strain.

a constant fiber volume fraction, the longer fiber added in the specimen results in a less amount of fibers, which would decrease the fiber pull-out and sliding events, on the other hand, the longer fiber has a larger fiber embedded length which would cause more fiber pull-out and sliding events. Therefore, there exists an optimal value of 280 for the fiber aspect ratio in this study when taking the two aspects into consideration.

4.3 Damage Mechanism

The failure pattern can be illustrated by AF (kHz) and RA value (ms/v) (Li et al. 2017). The AF is defined as a ratio of AE counts (number of threshold crossing) to duration for an elastic wave, and the RA is a tangent value of the rise time (ms) to the maximum amplitude (V), as shown in Fig. 11a. It has been well confirmed that a shear crack occurs when the signal has a high RA value and a low
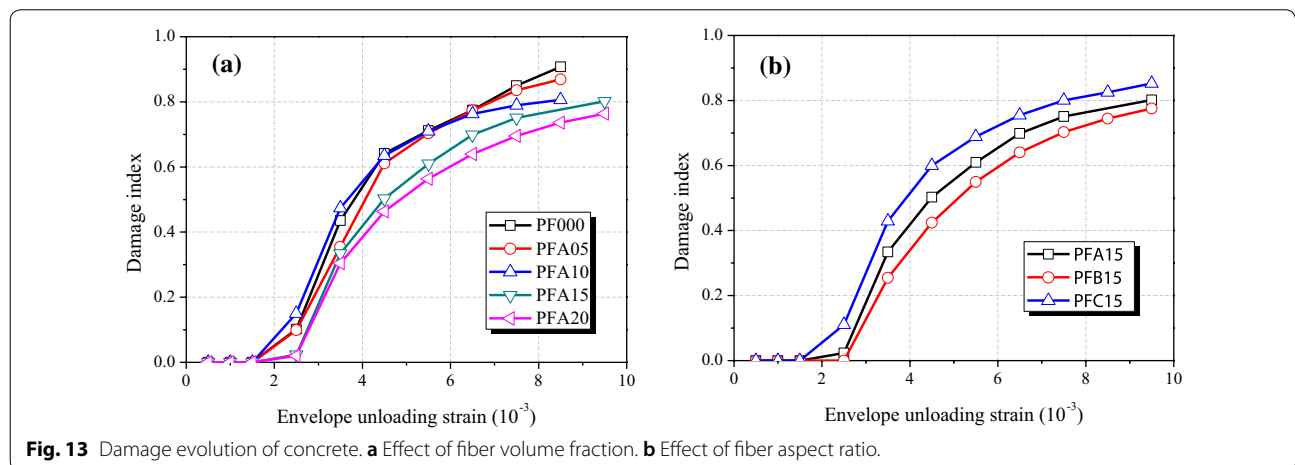
Fig. 13 Damage evolution of concrete. **a** Effect of fiber volume fraction. **b** Effect of fiber aspect ratio.

Xu *et al. Int J Concr Struct Mater* (2018) 12:68

Page 14 of 20

Fig. 15 Cumulative AE hits for PFRC under monotonic loading. **a** Effect of fiber volume fraction. **b** Effect of fiber aspect ratio.

AF value, while a tensile crack signal owns a low RA value and a high AF (Li et al. 2017). The crack classification method is schematically shown in Fig. 11b.

Figure 16 shows the typical classification of cracks in concrete under monotonic compression. The diagonal line plotted in each figure is the transition line between tensile cracks and shear cracks. It is noted that the AF for all specimens is 0–100 kHz and the RA values are up to 1400 ms/V. Both tensile and shear cracks are detected for plain concrete and PFRC. However, comparing the two figures, it is easily observed that for plain concrete, the tensile cracks are more than shear cracks, while, for PFRC, the proportion of shear cracks to the total is larger than that of plain concrete. The AF of the tensile cracks in PFRC is almost less than 60 kHz, which has a big difference from plain concrete (see in Fig. 16a). The above observations indicate that the tensile cracks determine the failure pattern of plain concrete, while shear cracks are the main contributors to dominate the failure
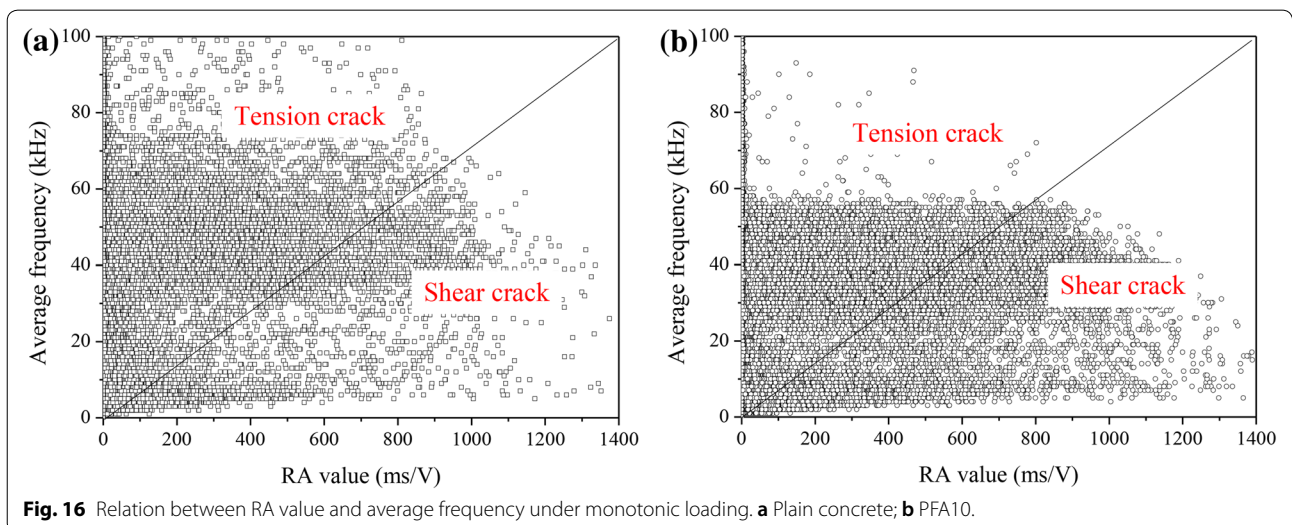
behavior of PFRC. The finding is in consistent with the macro failure patterns (see in Fig. 3).

5 Constitutive Model for PFRC
5.1 Monotonic Stress–Strain Model
The experimental study showed that the stress–strain curves of PFRC are similar to that of plain concrete, which can be clearly divided into two distinct segments. Therefore, the monotonic stress–strain model for plain concrete can be applicably modified for PFRC. At present, many forms of equations for stress–strain curve of plain concrete has been suggested. In this study, in order to connecting to the Chinese Code GB 50010-2010 (2010) and applying conveniently, the elastic damage model suggested by GB 50010-2010 (2010) is employed as the basis, the equation of which is written as:

$$\sigma = (1 - d)E_c\varepsilon \tag{3}$$

Fig. 16 Relation between RA value and average frequency under monotonic loading. **a** Plain concrete; **b** PFA10.

where, σ is the stress, ε is the strain, d is the scalar elastic damage index ranging from 0 to 1, E_c is the initial elastic modulus. The formulations of d are given as:

$$d = \begin{cases} 1 - \frac{\rho_c n}{n - 1 + x^n} & (x \leq 1) \\ 1 - \frac{\rho_c}{\alpha_c (x-1)^2 + x} & (x > 1) \end{cases} \quad (4)$$

$$x = \frac{\varepsilon}{\varepsilon_{cu}}, \ \rho_c = \frac{f_c}{E_c \varepsilon_{cu}}, \ n = \frac{1}{1 - \rho_c} \quad (5)$$

where, x is the normalized strain, ρ_c is the strength degradation factor corresponding to the peak stress, α_c is a parameter controlling the curvature of the descending branch of the stress–strain curve.

For a damage elasto-plastic model, the model equation can be written as (see in Fig. 17):

$$\sigma = (1 - D)E_c(\varepsilon - \varepsilon_{pl}) \quad (6)$$

Herein, D is the elasto-plastic damage variant, which can be seemed as the ratio of secant unloading stiffness degradation, as shown in Eq. (7):

$$D = 1 - \frac{E_{un}}{E_c} \quad (7)$$

where, E_{un} is the secant unloading stiffness for each loading cycle. ε_{pl} is the plastic strain, the formulation of which is given as:

$$\varepsilon_{pl} = \varepsilon_{un} - \frac{(\varepsilon_{un} + \varepsilon_{ca})\sigma_{un}}{\sigma_{un} + E_c \varepsilon_{ca}} \quad (8)$$

$$\varepsilon_{ca} = \max\left(\frac{\varepsilon_{cu}}{\varepsilon_{cu} + \varepsilon_{un}}, \frac{0.09\varepsilon_{un}}{\varepsilon_{cu}}\right)\sqrt{\varepsilon_{cu}\varepsilon_{un}} \quad (9)$$

Combined the Eqs. (3), (6), (8, 9), the format of D can be obtained as:

$$D = \frac{\varepsilon}{\varepsilon + \varepsilon_{ca}}d \quad (10)$$

In Eq. (10), ε_{ca} is the additional strain defined as the strain at the intersection of the initial tangent and the plastic unloading secant slope (Mander et al. 1988), which can be calculated following Eq. (9). However, from Eqs. (9) and (10), it can be observed that the damage decreases during the final loading process, which is not in consistency with the limitation of damage variant from 0 to 1. The main reason for that is owing to the formulation of ε_{ca} is not clear and precise. In order to overcome the issue, a function is developed by Ren and Li (2015) based on the two sectional type of functions were suggested by Mander et al. (1988), and shown as:

$$\varepsilon_{ca} = \frac{\varepsilon_{cu}}{\varepsilon_{cu} + \varepsilon}\sqrt{\varepsilon_{cu}\varepsilon} = \frac{\sqrt{x}}{1 + x}\varepsilon_{cu} \quad (11)$$

Therefore, the equation of D changes as:

$$D = \frac{x(1 + x)}{x(1 + x) + \sqrt{x}}d \quad (12)$$

In the present model, only E_c, f_{cu}, ε_{cu}, ε_{pl} and α_c are necessary model parameters. However, results in current and previous studies show that PF has insignificant effect

Fig. 17 Stress–strain model for PFRC. **a** Monotonic loading; **b** Cyclic loading.
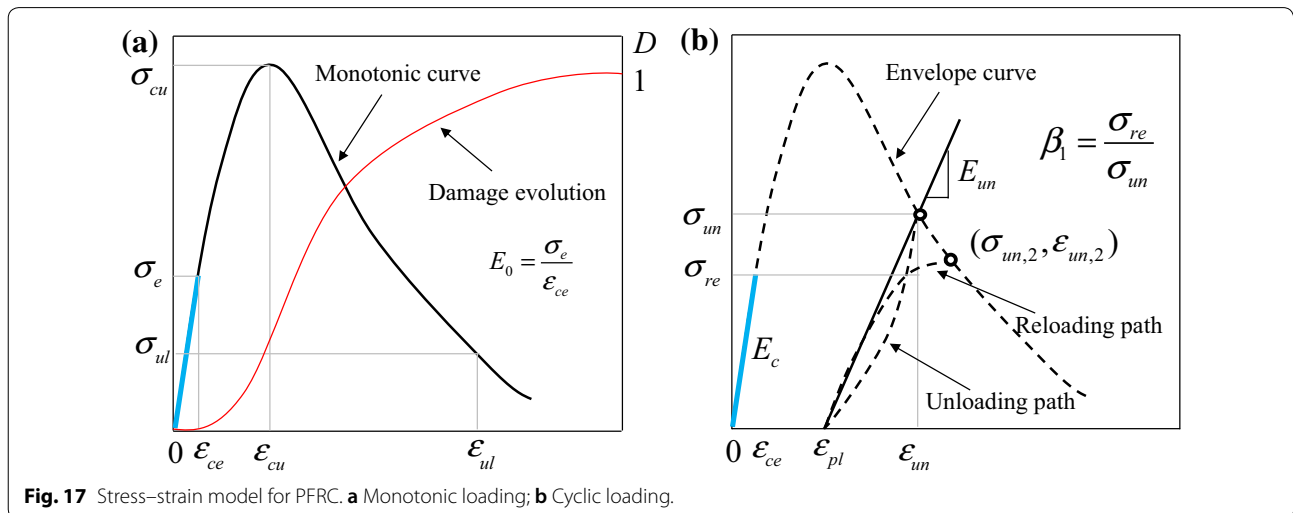
on the peak strength, peak strain as well as the elastic modulus, which are all almost the same as those of plain concrete, as shown in Fig. 18. The calculation of the elastic modulus of plain concrete can adopt the formulation suggested by Ren and Li (2015) in Eq. (13).

$$E_c = \frac{10^2}{2.2 + \frac{34.7}{f_{cu,k}}} \tag{13}$$

where, $f_{cu,k}$ is the standard value of compressive strength. As is well known, α_c is related to the fiber characteristic parameter ($\lambda_f = V\% \times l_f/d_f$) (Chi et al. 2014). Based on a regression analysis of the fitting results, α_c is obtained in Eq. (14). The comparison results between fitting and predicted results are shown in Fig. 18d.

$$\alpha_c = 1.101 + 0.79e^{-3.308\lambda_f} \tag{14}$$

5.2 Cyclic Stress–Strain Model

According to GB 50010-2010 (2010), the unloading and reloading branch can be assumed as a bias line. This assumption is easy to be adopted in application in the analysis of engineering structures, which is also employed in this study. The equations for unloading and reloading paths are shown in Eqs. (15, 16).
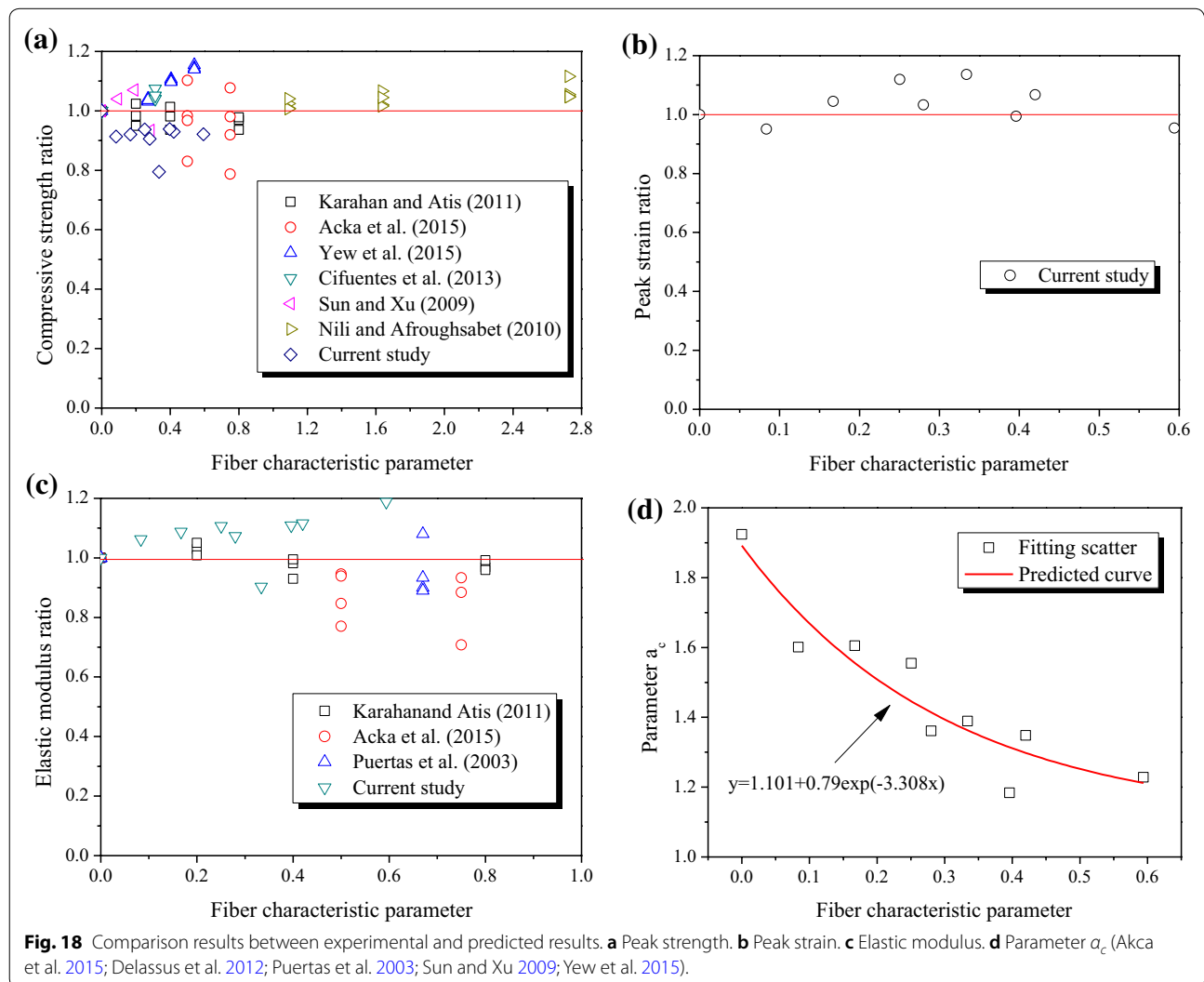
$$\sigma = E_{un}(\varepsilon - \varepsilon_{pl}) \tag{15}$$

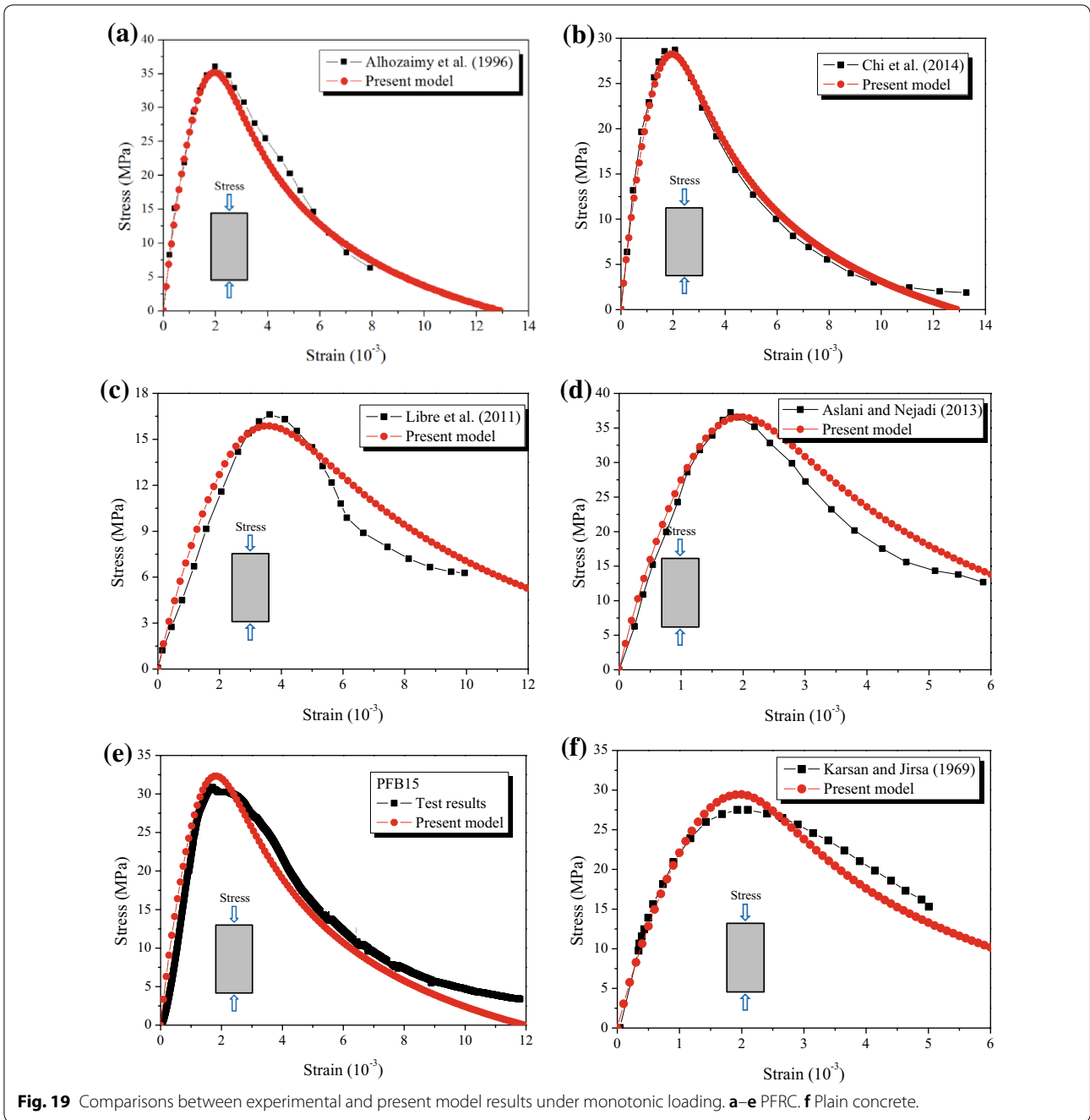$$E_{un} = \frac{\sigma_{un}}{\varepsilon_{un} - \varepsilon_{pl,un}} \tag{16}$$

where, the plastic strain ε_{pl} is calculated by Eq. (1).

5.3 Evaluation of the Proposed Model

Figures 19 and 20 show the typical comparisons of the models' predictions and test results in current independent results and open literatures under monotonic and cyclic compressive loading, respectively. The key

Fig. 18 Comparison results between experimental and predicted results. **a** Peak strength. **b** Peak strain. **c** Elastic modulus. **d** Parameter α_c (Akca et al. 2015; Delassus et al. 2012; Puertas et al. 2003; Sun and Xu 2009; Yew et al. 2015).

Xu *et al. Int J Concr Struct Mater* (2018) 12:68

Page 17 of 20

Fig. 19 Comparisons between experimental and present model results under monotonic loading. **a**–**e** PFRC. **f** Plain concrete.
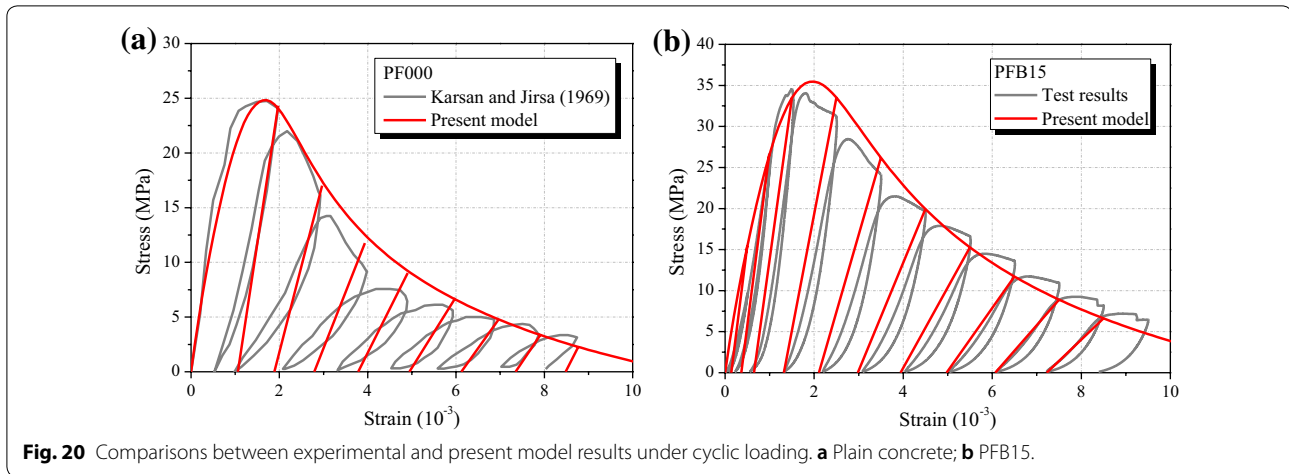
mechanical parameters needed in the model verification for each case are listed in Table 5. It is evident that the present model can provide fairly good estimation of the stress–strain response of PFRC, with slight discrepancies.

6 Conclusions

The main conclusions extracted from the present study are the following:

1. PF has a positive effect on the monotonic and cyclic compressive stress–strain behavior of concrete due to fiber crack arresting and bridging effect, mainly for the post-cracking branch. The monotonic loading curve of PFRC lies closely to the envelope curve of cyclic stress–strain response. Moreover, PF has little influence on the plastic strain accumulation, but improves the energy dissipated capacity and alleviates the performance degradation in terms of elastic

Xu *et al. Int J Concr Struct Mater* (2018) 12:68

Page 18 of 20

Fig. 20 Comparisons between experimental and present model results under cyclic loading. **a** Plain concrete; **b** PFB15.

Table 5 Key mechanical parameters used in the model verification.

No.	Literatures	Specimen	Dimension (mm)	V (%)	l/d	f_c (MPa)	ε_{cu} (10^{-3})
Monotonic loading							
(a)	Alhozaimy et al. (1996)	Cylinder	Φ152 × 305	0.2	400	42.35	2.05
(b)	Chi et al. (2014)	Prism	150 × 150 × 300	0.1	167	28.35	1.96
(c)	Libre et al. (2011)	Cylinder	Φ150 × 300	0.4	750	16.52	3.64
(d)	Aslani and Nejadi (2013)	Cylinder	Φ150 × 300	0.55	76.5	37.22	1.92
(e)	Current study	Prism	150 × 150 × 300	0.15	280	32.43	1.78
(f)	Karsan and Jirsa (1969)	Cylinder	Φ150 × 300	–	–	27.51	2.02
Cyclic loading							
(a)	Karsan and Jirsa (1969)	Cylinder	Φ150 × 300	–	–	24.62	1.75
(b)	Current study	Prism	150 × 150 × 300	0.15	280	32.41	1.78

stiffness and strength, especially at the peak-stress region. Furthermore, the effect of fiber volume fraction on the cyclic stress–strain behavior of concrete shows more pronounced than that of fiber aspect ratio.

2. The compressive toughness and ultimate strain are enhanced by the incorporation of fibers. Both of them increase with the increasing fiber volume fraction (up to 0.15%), while, for the fiber aspect ratio, they increase first and decrease afterwards when the aspect ratio changes from 167 to 396. However, PF has no significant effects on the modulus of elasticity, compressive strength and the peak strain.

3. The damage has a quick evolution just after the peak stress, at which the AE hits have a concentrate release, with an obvious drop in the axial load. Moreover, the damage of PFRC is mainly driven by the strain of envelope curve based on an analysis from elastic stiffness degradation process. In addition, the total AE activities of PFRC is higher than that of plain concrete due to fiber pull-out and fiber sliding

events, and the cumulative AE hits increase with the increasing fiber volume fraction, but reach the largest amount with the fiber aspect ratio of 280 at the same fiber content.

4. All concrete specimens exhibit both tensile and shear cracks. The proportion of shear crack in PFRC is larger than that in plain concrete. The failure behavior of PFRC is dominated by shear cracking mode, while for plain concrete, tensile cracks are the primarily actor in failure mode determination.

5. A damage elasto-plastic constitutive model is developed to generate both the monotonic and cyclic compressive stress–strain behavior of PFRC connecting to the Chinese Code GB 50010-2010. The predictions are found in satisfactory agreement with the results in present study and other open literatures.

Authors' contributions
LX and BL drafted the manuscript. BL, CL, BH and YS conducted the experiment of cyclic compression on the concrete specimens. YC and XD helped to improve the quality of the manuscript. All authors read and approved the final manuscript.

Author details
[1] School of Civil Engineering, Wuhan University, 8 Dong Hu South Road, Wuhan 430072, China. [2] Imperial College London, South Kensington, London SW72AZ, UK.

Competing interests
The authors declare that they have no competing interests.

Publisher's Note
Springer Nature remains neutral with regard to jurisdictional claims in published maps and institutional affiliations.

References
Abbasnia, R., & Ziaadiny, H. (2010). Behavior of concrete prisms confined with FRP composites under axial cyclic compression. *Engineering Structures, 32*(3), 648–655.

Aggelis, D. G., Soulioti, D. V., Sapouridis, N., Barkoula, N. M., Paipetis, A. S., & Matikas, T. E. (2011). Acoustic emission characterization of the fracture process in fibre reinforced concrete. *Construction and Building Materials, 25*(11), 4126–4131.

Akca, K. P., Cakir, O., & Ipek, M. (2015). Properties of polypropylene fiber reinforced concrete using recycled aggregates. *Construction and Building Materials, 98,* 620–630.

Alhozaimy, A. M., Soroushia, P., & Mirza, F. (1996). Mechanical properties of polypropylene fiber reinforced concrete and the effects of Pozzolanic materials. *Cement and Concrete Composites, 18*(2), 85–92.

Aslani, F., & Nejadi, S. (2013). Self-compacting concrete incorporating steel and polypropylene fibers: Compressive and tensile strengths, moduli of elasticity and rupture, compressive stress–strain curve, and energy dissipated under compression. *Composites: Part B, 53,* 121–133.

Bahn, B. Y., & Hsu, C. T. T. (1988). Stress–strain behavior of concrete under cyclic loading. *ACI Materials Journal, 95*(2), 178–193.

Brandt, A. M. (2008). Fibre reinforced cement-based (FRC) composites after over 40 years of development in building and civil engineering. *Composite Structures, 86,* 3–9.

Breccolotti, M., Bonfigli, M. F., D'Alessandro, A., & Materazzi, A. L. (2015). Constitutive modeling of plain concrete subjected to cyclic uniaxial compressive loading. *Construction and Building Materials, 94,* 172–180.

Caggiano, A., Gambarelli, S., Martinelli, E., Nisticò, N., & Pepe, M. (2016). Experiment characterization of the post-cracking response in hybrid steel/polypropylene fiber-reinforced concrete. *Construction and Building Materials, 125,* 1035–1043.

Campione, G., & Mendola, L. L. (2001). Stress–strain behavior in compression of lightweight fiber reinforced concrete under monotonic and cyclic loads. *Earthquake Resistant Engineering Structures, 57*(9), 387–396.

Chen, G. M., He, Y. H., Yang, H., Chen, J. F., & Guo, Y. C. (2014). Compressive behavior of steel fiber reinforced recycled aggregate concrete after exposure to elevated temperatures. *Construction and Building Materials, 128*(71), 1–15.

Chi, Y., Xu, L., & Zhang, Y. (2014). Experimental study on hybrid fiber-reinforce concrete subjected to uniaxial compression. *Journal of Materials in Civil Engineering, 26*(2), 211–218.

Cifuentes, H., & Garcfa, F. (2013). Influence of the properties of polypropylene fibres on the fracture behaviour of low-, normal- and high-strength FRC. *Construction and Building Materials, 45,* 130–137.

Dai, Q., Ng, K., Zhou, J., Kreiger, E. L., & Ahlborn, T. M. (2012). Damage investigation of single-edge notched beam tests with normal strength concrete and ultra high performance concrete specimens using acoustic emission techniques. *Construction and Building Materials, 31*(6), 231–242.

Dassios, K. G., Aggelis, D. G., Kordatos, E. Z., & Matikas, T. E. (2013). Cyclic loading of a SiC-fiber reinforced ceramic matrix composite reveals damage mechanisms and thermal residual stress state. *Composites: Part A, 44*(44), 105–113.

Delassus, G. S., Cho, H., Hoand, S., & Elceiri, G. L. (2012). Fracture behavior and damage evaluation of polyvinyl alcohol fiber concrete using acoustic emission technique. *Materials and Design, 40,* 205–211.

GB 50010-2010. *Code for design of concrete structures*. (2010). Ministry of House and Urban–Rural Development of People's Republic of China, China.

GB/T 50081-2002. (2002). Standard for test method of mechanical properties on ordinary concrete. Ministry of House and Urban–Rural Development of People's Republic of China, China.

Hasan, M., Afroz, M., & Mahmud, H. (2011). An experimental investigation on the mechanical behavior of macro synthetic fibre reinforced concrete. *International Journal of Civil and Environmental Engineering, 11*(03), 18–23.

He, W., Wu, Y. F., & Liew, K. M. (2008). A fracture energy based constitutive model for the analysis of reinforced concrete structures under cyclic loading. *Computer Methods in Applied Mechanics and Engineering, 197*(51), 4745–4762.

Huang, L., Chi, Y., Xu, L., Chen, P., & Zhang, O. (2016). Local bond performance of rebar embedded in steel-polypropylene hybrid fiber reinforced concrete under monotonic and cyclic loading. *Construction and Building Materials, 103,* 77–92.

JGJ 55-2011. 2011. Specification for mix proportion design of ordinary concrete. Ministry of House and Urban–Rural Development of People's Republic of China, China.

Jin, L., Li, D., & Du, X. (2016). Mechanical behavior and size effect of moderate high-strength RC columns under monotonic and cyclic axial compression. *Engineering Structures, 124,* 269–285.

Kakooei, S., Akil, H. M., Jamshidi, M., & Rouhi, J. (2012). The effects of polypropylene fibers on the properties of reinforced concrete structures. *Construction and Building Materials, 27*(1), 73–77.

Karahan, O., & Atis, C. D. (2011). The durability properties of polypropylene fiber reinforced fly ash concrete. *Materials and Design, 32*(2), 1044–1049.

Karsan, L. D., & Jirsa, J. O. (1969). Behavior of concrete under compression loadings. *Journal of Structural Division, 95*(12), 2543–2563.

Lam, L., & Teng, J. G. (2009). Stress–strain model for FRP-confined concrete under cyclic axial compression. *Engineering Structures, 31*(2), 308–321.

Lam, L., Teng, J. G., Cheung, C. H., & Xiao, Y. (2006). FRP-confined concrete under axial cyclic compression. *Cement and Concrete Composites, 28*(10), 949–958.

Lee, H. P., Awang, A. Z., & Omar, W. (2014). Steel strap confined high strength concrete under uniaxial cyclic compression. *Construction and Building Materials, 72*(1), 48–55.

Lee, J. K., & Lee, J. H. (2002). Nondestructive evaluation on damage of carbon fiber sheet reinforced concrete. *Composite Structures, 58*(1), 139–147.

Lee, Y. H., & Willan, K. J. (1997). Mechanical properties of concrete under cyclic compression. *ACI Materials Journal, 94,* 457–467.

Li, J., & Ren, X. (2009). Stochastic damage model for concrete based on energy equivalent strain. *Internation Journal of Solids and Structures, 46*(11), 2407–2419.

Li, B., Xu, L., Chi, Y., Huang, B., & Li, C. (2017). Experimental investigation on the stress–strain behavior of steel fiber reinforced concrete subjected to uniaxial compression. *Construction and Building Materials, 140,* 109–118.

Liang, Y., Sun, C., & Ansari, F. (2004). Acoustic emission characteristization of damage in hybrid fiber reinforced polymer rods. *Journal of Composites for Construction, 8*(1), 70–78.

Libre, N. A., Shekarchi, M., Mahoutian, M., & Soroushian, P. (2011). Mechanical properties of hybrid fiber reinforced lightweight aggregate concrete made with natural pumice. *Construction and Building Materials, 25*(5), 2458–2464.

Maekawa, K., & El-Kashif, K. F. (2004). Cyclic cumulative damaging of reinforced concrete in post-peak regions. *Journal of Advanced Concrete Technology, 2*(2), 257–271.

Mander, J. B., Priestley, M. J. N., & Park, R. (1988). Theoretical stress–strain model for confined concrete. *Journal of Structural Engineering, 114*(8), 1804–1826.

Mazaheripour, H., Ghanbarpour, S., Mirmoradi, S. H., & Hosseinpour, I. (2011). The effect of polypropylene fibers on the properties of fresh and hardened lightweight self-compacting concrete. *Construction and Building Materials, 25*(1), 351–358.

Neuenschwander, M., Knobloch, M., & Fontana, M. (2016). Suitability of the damage-plasticity modeling concept for concrete at elevated temperatures: Experimental validation with uniaxial cyclic compression tests. *Cement and Concrete Research, 79,* 57–75.

Nili, M., & Afroughsabet, V. (2010). The effects of silica fume and polypropylene fibers on the impact resistance and mechanical properties of concrete. *Construction and Building Materials, 24*(6), 927–933.

Nobili, A., Lanzoni, L., & Taratino, A. M. (2013). Experimental investigation and monitoring of a polypropylene-based fiber reinforced concrete road pavement. *Construction and Building Materials, 47*(10), 888–895.

Osorio, E., Bairan, J. M., & Mari, A. R. (2013). Lateral behavior of concrete under uniaxial compressive cyclic loading. *Materials and Structures, 46*(5), 709–724.

Otter, D. E., & Naaman, A. E. (1988). Properties of steel fiber reinforced concrete under cyclic load. *ACI Materials Journal, 85*(4), 254–261.

Parveen, A. S. (2013). Structural behavior of fibrous concrete using polypropylene fibres. *International Journal of Modern Engineering Research, 3*(3), 1279–1282.

Puertas, F., Amat, T., Fernandez-Jimenez, A., & Vazquez, T. (2003). Mechanical and durable behavior of alkaline cement mortars reinforced with polypropylene fibres. *Cement and Concrete Research, 33*(12), 2031–2036.

Ren, X., & Li, J. (2015). Calculation of concrete damage and plastic deformation. *Building Structure, 45*(2), 29–32. **(in Chinese)**.

Sakai, J., & Kawashima, K. (2006). Unloading and reloading stress–strain model for confined concrete. *Journal of Structural Engineering, 132*(1), 112–122.

Sinaie, S., Heidarpour, A., Zhao, X. L., & Sanjayan, J. G. (2015). Effect of size on the response of cylindrical concrete samples under cyclic loading. *Construction and Building Materials, 84,* 399–408.

Sinha, B. P., Gerstle, K. H., & Tulin, L. G. (1964). Stress–strain relations for concrete under cyclic loading. *ACI Structural Journal, 61*(2), 195–211.

Song, P. S., Hwang, S., & Sheu, B. C. (2005). Strength properties of nylon- and polypropylene-fiber-reinforced concretes. *Cement and Concrete Research, 35*(8), 1546–1550.

Soulioti, D., Barkoula, N. M., Paipetis, A., Matikas, T. E., Shiotani, T., & Aggelis, D. G. (2009). Acoustic emission behavior of steel fibre reinforced concrete under bending. *Construction and Building Materials, 23*(12), 3532–3536.

Suaris, W., Ouyang, C., & Fernando, V. M. (1990). Damage model for cyclic loading of concrete. *Journal of Engineering Mechanics, 116*(5), 1020–1035.

Sun, Z., & Xu, Q. (2009). Microscopic, physical and mechanical analysis of polypropylene fiber reinforced concrete. *Materials Science and Engineering A, 527*(1), 198–204.

Swit, G. (2004). Evaluation of compliance changes in concrete beams reinforced by glass fiber reinforced plastics using acoustic emission. *Journal of Materials in Civil Engineering, 16*(5), 414–418.

Tangawa, Y., & Hatanaka, S. (1983). Stress–strain relations of steel fiber reinforced concrete under repeated compressive load. *Cement and Concrete Research, 13*(6), 801–808.

Wang, Z. Y., Wang, D. Y., Smith, S. T., & Lu, D. G. (2012). CFRP-confined square RC columns. I:Experimental investigation. *Journal of Composites for Construction, 16*(2), 150–160.

Watanabe, T., Nishibata, S., Hashimoto, C., & Ohtsu, M. (2007). Compressive failure in concrete of recycled aggregate by acoustic emission. *Construction and Building Materials, 21*(3), 470–476.

Yankelevsky, D. Z., & Rainhardt, H. W. (1989). Uniaxial behavior of concrete under cyclic loading. *Journal of Engineering Structures, 115*(1), 166–182.

Yew, M. K., Mahmud, H. B., Ang, B. C., & Ming, C. Y. (2015). Influence of different types of polypropylene fibres on the mechanical properties of high-strength oil palm shell lightweight concrete. *Construction and Building Materials, 90,* 36–43.

Yin, S., Tuladhar, R., Collister, T., Combe, M., Sivakugan, N., & Deng, Z. (2015). Post-cracking performance of recycled polypropylene fibre in concrete. *Construction and Building Materials, 101*(1), 1069–1077.

Zhang, P., & Li, Q. (2013). Effect of polypropylene fiber on durability of concrete composite containing fly ash and silica fume. *Composites: Part B, 45*(1), 1587–1597.

Zhang, H., Liu, Y., Sun, H., & Wu, S. (2016). Transient dynamic behavior of polypropylene fiber reinfo rced mortar under compressive impact loading. *Construction and Building Materials, 111,* 30–42.